第 49 卷 第 20 期/2022 年 10 月/中国激光 研究论文

中国激光

激光眼底手术传热特性数值模拟研究

赵鹏辉[1]，赵一博[1]，李东[1*]，陈斌[1]，姚亮[2**]

[1]西安交通大学动力工程多相流国家重点实验室，陕西 西安 710049

[2]西安交通大学第二附属医院眼科，陕西 西安 710004

摘要 激光热疗是多种眼底视网膜疾病的首选疗法。然而，激光参数选取不当造成的感光细胞损伤概率可达 50% 以上。构建准确的全眼三维传热模型可为临床医生选取激光参数提供依据。为此，本团队基于真实眼球结构建立了全眼宏观传热模型，通过数值模拟分析了人眼外部环境、眼前部组织吸收和脉络膜血流灌注对激光手术过程中眼底温度分布的影响。结果显示：角膜与环境间的对流换热会导致眼球温度发生变化，但对眼底手术的影响较小；在临床常用的 450～900 nm 波段内，不考虑眼前部组织对激光能量的吸收时，眼底各层温升误差可达 24%；脉络膜血流灌注项对激光手术中眼球温度分布的影响主要取决于脉宽，经瞳孔温热疗法下考虑和忽略脉络膜血流灌注效应时眼底温升分别为 11.54 ℃和 21.15 ℃，计算误差可达 83%。

关键词 医用光学；激光；眼底疾病；光热效应；生物传热；血流灌注

中图分类号 R318.51；R774.1 **文献标志码** A **DOI**：10.3788/CJL202249.2007101

1 引 言

眼睛是人类最重要的感觉器官，大脑中 80% 的知识和记忆都是通过眼睛获取的[1]。眼底，即眼球后部组织，是光信号在大脑中形成图像的核心区域，由视网膜（神经上皮层、视网膜色素上皮层）、脉络膜及巩膜构成。眼底病是发生在眼底的一系列眼疾的总称，包括糖尿病视网膜病变[2]、视网膜中央静脉阻塞[3]、老年黄斑变性[4]等。眼底病已被世界卫生组织列为三大致盲性眼病首位，占全部致盲眼病的 54.7%，是老年人最主要的致盲因素[5]。

眼底位于眼球后方，传统的手术方法难以实施。激光热疗具有非接触、简便、快捷的优点[6]。基于生物组织的选择性光热效应[7-8]，激光可以通过热凝结封闭视网膜渗漏血管，通过热刺激修复色素上皮层传质功能，还可以吸收渗液消除黄斑水肿，最终达到治疗效果。然而，在临床治疗中，由于激光参数选取不当造成的视网膜感光组织热损伤概率达到了 50%以上[9]。采用数值模拟对眼底激光手术的热过程进行仿真，有望为临床医生选取激光参数提供依据，进而提高手术的安全性和有效性。

Taflove 等[10]和 Emery[11]等于 1975 年提出了二维眼球传热模型，并计算了微波辐射下眼球内的温度分布。Ng 等[12]、Cvetković 等[13]和 Narasimhan 等[14]利用更为精细的三维模型模拟了激光作用下眼底的光热转化过程。然而，上述研究仅考虑了巩膜血液流动对眼球传热的影响，忽略了眼球内部的脉络膜血液灌流效应。鉴于此，本团队基于 Pennes 生物传热方程构建全眼数值计算模型，计算稳态及激光加热下眼球内的热响应过程，分析眼球前部组织的光吸收以及脉络膜血液灌流对不同时间尺度激光手术过程的影响，以期为临床治疗提供了重要的理论指导。

2 数理模型

本文采用的全眼三维模型切面图如图 1 所示。该模型将整个眼球简化为 8 个区域，沿 z 轴负方向依次为角膜、前后房、虹膜、晶状体、玻璃体等眼球前部组织以及由视网膜、脉络膜、巩膜组成的眼底。眼球沿瞳孔轴的横向直径为 24 mm，眼球关于瞳孔轴（垂直于角膜表面）对称，后半部分近似球形。激光照射下的眼球内传热过程可由 Pennes 生物传热方程表示，即

$$\rho c_p \frac{\partial T}{\partial t} = \nabla(k\ \nabla T) + Q_b + Q_m + Q, \tag{1}$$

其中，

$$Q_b = \omega_b c_b (T_{in} - T_{out}), \tag{2}$$

式中：ρ 为生物组织的密度，单位为 kg·m^{-3}；c_p 为生物组织的比热容，单位为 J·kg^{-1}·K^{-1}；k 为组织的热导率，单位为 W·m^{-1}·K^{-1}；T 为组织温度，单位为 K；Q_m 为组织的代谢产热率，单位为 W·m^{-3}；Q_b 为脉络膜血流灌注产生的对流冷却效应，单位为 W·m^{-3}；ω_b 为脉络膜血液灌注率，ω_b=0.233 kg·m^{-3}·s^{-1}[15]；

收稿日期：2022-03-25；**修回日期**：2022-04-15；**录用日期**：2022-04-19

基金项目：国家自然科学基金（51976170）

通信作者：*lidong@mail.xjtu.edu.cn；**lyao0815@163.com

c_b 为血液比热容，单位为 J·kg^{-1}·K^{-1}；T_{in} 为动脉入口的血液温度，单位为 K；T_{out} 为静脉出口的血流温度，单位为 K；Q 为激光照射时各层组织单位体积内单位时间内吸收的能量，单位为 W·m^{-3}，可由 Kubelka-Munk 模型[16]计算得到。

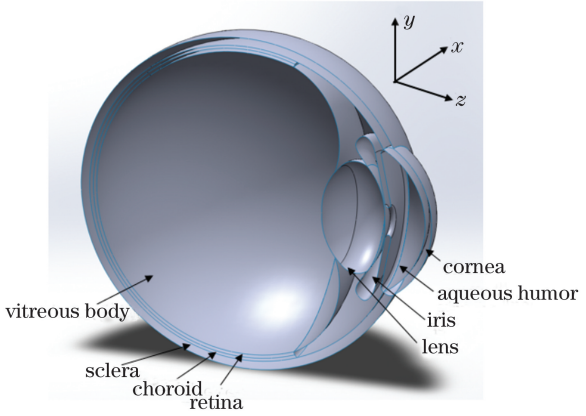

图 1 简化的眼球三维模型剖面图

Fig. 1 Section of simplified three-dimensional model of eyeball

因眼球各组织层均为高散射组织，且眼球前部的角膜、房水、晶状体、玻璃体等结构对激光能量的吸收很少，故本文采用 Kubelka-Munk 模型模拟眼球内激光通量的分布。眼球内不同组织层的衰减系数不同，并且激光能量已经在前一层中被部分吸收，所以对于不同的组织层，每一层激光入射强度 $I_{\lambda,0}$ 不同，而且距离激光入射位置越远的组织层，其初始激光入射强度 $I_{\lambda,0}$ 越小。

在眼底激光手术中，光斑直径(50～500 μm)与眼球直径(24 mm)相差几个数量级。为计算方便，这里假设激光光束截面光强均匀分布，即同一横截面内光强相同。由于径向的强度均匀，这里假定眼球组织的热源为

$$Q=\mu_a\cdot I_{\lambda,0}\exp\left[-(\mu_a+(1-g)\mu_s)z\right],\quad(3)$$

式中：μ_a 为组织吸收系数；μ_s 为组织散射系数；g 为组织各向异性因子。由于激光光束沿瞳孔轴(z 轴)入射，激光并不会照射虹膜，因此虹膜组织中没有激光通量。

激光在光传播方向(z 轴径向)上均匀分布。当 $z=0$ 时，角膜边界的激光入射强度为

$$I_{\lambda,0}=\frac{E_0}{R^2\pi},\quad(4)$$

式中：E_0 为激光器的输出能量密度，单位为 J·cm^{-2}；R 为角膜上的光束半径，单位为 μm。本文忽略晶状体的聚焦作用，故沿瞳孔轴的光束半径保持不变，见图 2。

模型的边界条件如图 2 所示。在眼球后方，巩膜向周围散热的计算公式为

$$k\frac{\partial T}{\partial \boldsymbol{n}}=h_b(T-T_b),\quad(5)$$

式中：h_b 为巩膜与眼球后方组织间的对流换热系数，其值为 65 W·m^{-2}·K^{-1}[17]；T_b 为人体体核温度，37 ℃；$\boldsymbol{n}$ 是垂直于巩膜表面的法线向量，表示由血液与周围组织温度梯度引起的热通量。

在角膜表面，边界条件需考虑自然对流、辐射和泪液蒸发，因此可得

$$k\frac{\partial T}{\partial \boldsymbol{n}}=h_a(T-T_a)+\varepsilon\sigma(T^4-T_a^4)+E_a,\quad(6)$$

式中：E_a 为角膜泪液蒸发速率[15]，其值为 40 W·m^{-2}；σ 为 Stefan-Boltzmann 常数，其值为 5.67×10^{-8} W·m^{-2}·K^{-4}；h_a 为外界空气与眼球之间的对流换热系数[17]，其值为 10 W·m^{-2}·K^{-1}；T_a 为环境温度；ε 为组织发射率。

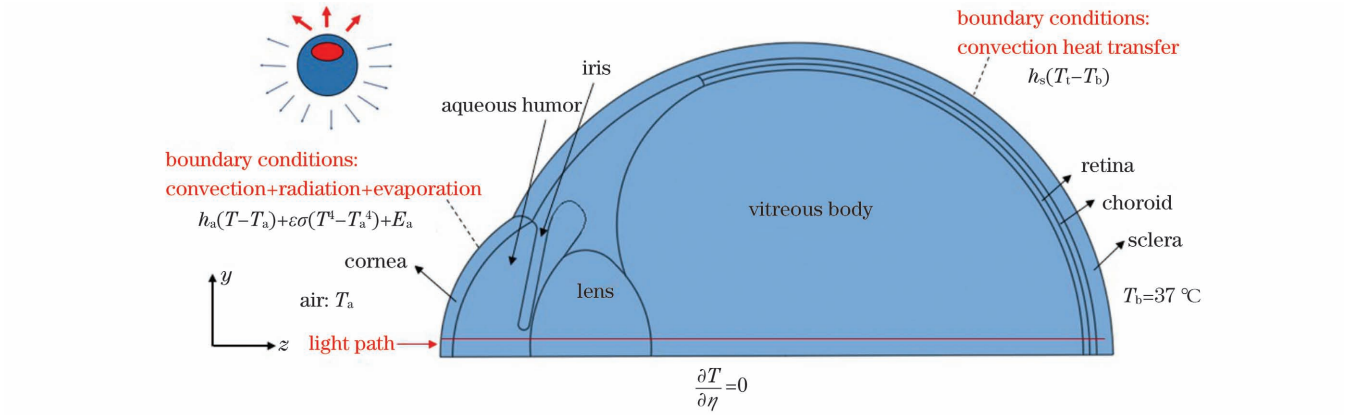

图 2 模型边界条件示意图

Fig. 2 Schematic of model boundary conditions

基于 ANSYS ICEM 对整个眼球进行四面体网格划分。在角膜、视网膜、脉络膜、巩膜等较薄组织内采用精密网格，在玻璃体、晶状体等较厚组织内采用稀疏网格，模型中组织区域之间为耦合边界条件，在任意两个组织层之间的界面处，保持温度和热通量的连续性。经过网格无关性验证，最终使用 229 万个四面体网格，如图 3 所示。基于 Fluent 6.3.26 采用有限容积法求解上述控制方程。整个眼球的初始温度设定为 37 ℃。在眼球模型中，假设每个区域均具有均匀的物性参数和光学参数。各组织层的主要几何参数、物性参数及光学参数分别如表 1 和表 2 所示。

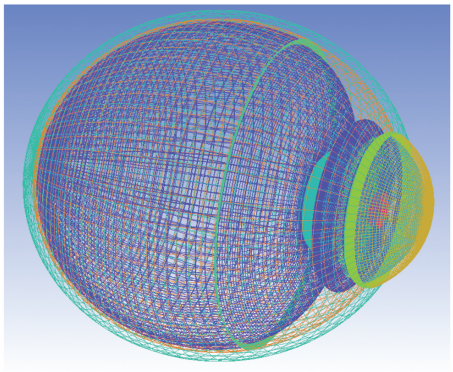

图 3 全眼模型网格划分示意图

Fig. 3 Schematic of whole eye mesh

表 1 三维眼球模型各区域的几何参数和物性参数[15,18-19]

Table 1 Geometric and physical parameters of each region of three-dimensional eyeball model[15,18-19]

Tissue	Specific heat c_p/(J·kg^{-1}·K^{-1})	Density ρ/(kg·m^{-3})	Thermal conductivity k/(W·m^{-1}·K^{-1})	Anisotropy index g	Thickness H/mm
Cornea	4178	1050	0.580	0.9	0.45
Aqueous humor	3997	996	0.578	0.9	2.8
Iris	3340	1100	0.498	0.98	0.35
Lens	3997	1050	0.4	0.9	4.25
Vitreous	3997	1000	0.594	0.9	15.34
Retina	4178	992	0.565	0.97	0.21
Choroid	4178	1100	0.53	0.9325	0.25
Sclera	4178	1100	0.580	0.9	0.7

表 2 不同激光波长下各组织的光学参数[13,20]

Table 2 Optical parameters of each tissue at different laser wavelengths[13,20]

Tissue	Absorption coefficient μ_a/m^{-1}		Scattering coefficient μ_s/m^{-1}	
	532 nm	810 nm	532 nm	810 nm
Cornea	61.3	33.22	2268	1050
Aqueous humor	13.4	10.4	102	66.38
Iris	3.28	3.29	113.83	105.22
Lens	1.78	3.1	5.0	15.3
Retina	2900	767.1	26113	18792.2
Choroid	14385	760	52450	31945
Sclera	310.2	19.8	67980	29270

3 模拟结果与讨论

3.1 眼球稳态温度分布特性

为验证模型的正确性，本团队首先模拟了稳态条件下眼球的温度分布，并将其与经典文献结果进行了对比，对比结果如图 4 所示。从图 4 中可以看出，本文模拟结果与 Cvetković 等[13]的计算结果吻合得较好，验证了本模型的正确性。

随后，本团队研究了不同环境温度（T_a=0，10，25，35 ℃）对眼球内温度分布的影响。4 种环境温度下眼球内温度沿瞳孔轴的分布如图 5 所示。由于环境温度较低，眼球前部组织的温度低于眼底组织的温度。环境温度对眼球内稳态温度的分布具有显著影响。当 T_a=0 ℃时，角膜与眼球内部区域的温差可达到 5 ℃。

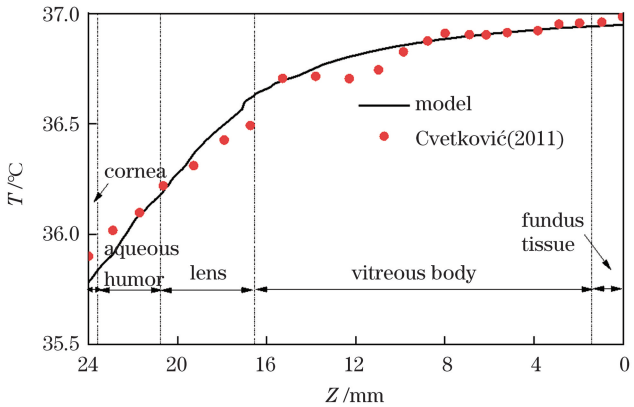

图 4 环境温度 25 ℃下本模型的温度分布与文献[13]计算结果的比较

Fig. 4 Comparison of temperature distribution between our model and reference[13] at ambient temperature of 25 ℃

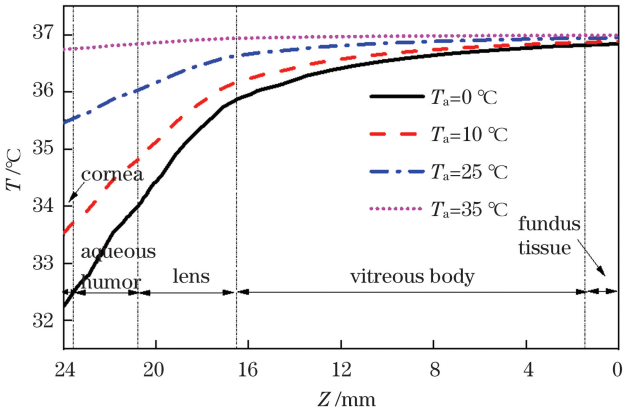

图 5 不同环境温度下眼球温度沿瞳孔轴的变化

Fig. 5 Changes of eyeball temperature with pupillary axis at four different ambient temperatures

即使环境温度为 0 ℃，眼底视网膜温度仅发生轻微变化(与 35 ℃环境温度下的眼底视网膜温度相比)，因此，外界环境温度引起的眼球温度场变化并不会对眼底激光手术产生影响。

3.2 眼球前部组织光吸收对眼底激光手术的影响

为方便建模，目前的研究往往会忽略眼球前部 4 个区域对激光能量的吸收和散射作用[14,21]。尽管眼球前部组织对光的吸收和散射作用较弱(见表 2)，但该部分组织位于激光入射光路的前段，且体积占比较大，因此，该部分组织的光吸收对眼底热效应的影响值得研究。本文选取两种典型眼底手术常用激光波长 532 nm 和 810 nm 进行分析。在这两种波长激光的照射下，瞳孔轴线上的温度分布如图 6 所示。两种波长激光的入射能量密度均为 5 J·cm^{-2}，激光脉宽 t_p=0.1 s，光束半径 r=200 μm。从图 6 中可以看出：虽然有近 20%的光能被眼球前部组织吸收，但由于前部组织的体积较大，因而温升较小，约为 0.3 ℃，不会对手术的安全性产生影响；但在眼底视网膜处，其温度受眼球前部光能吸收的影响较大。在考虑眼球前部四层组织吸收和散射特性的情况下，532 nm 和 810 nm 激光照射后视网膜的温度峰值分别为 49 ℃和 40.6 ℃，相比不考虑眼球前部组织吸收时分别降低了 3.8 ℃和 4.6 ℃，眼底温升误差最大值分别为 24%和 56%(考虑眼球前部组织吸收与否时二者温升的差值与不考虑眼球前部组织吸收时温升的比值)，会极大地影响整个眼底激光手术模拟计算的准确性。因而，为了确保激光眼底手术模拟的准确性，模拟计算时应该考虑眼球前部组织对激光能量的吸收和散射作用。

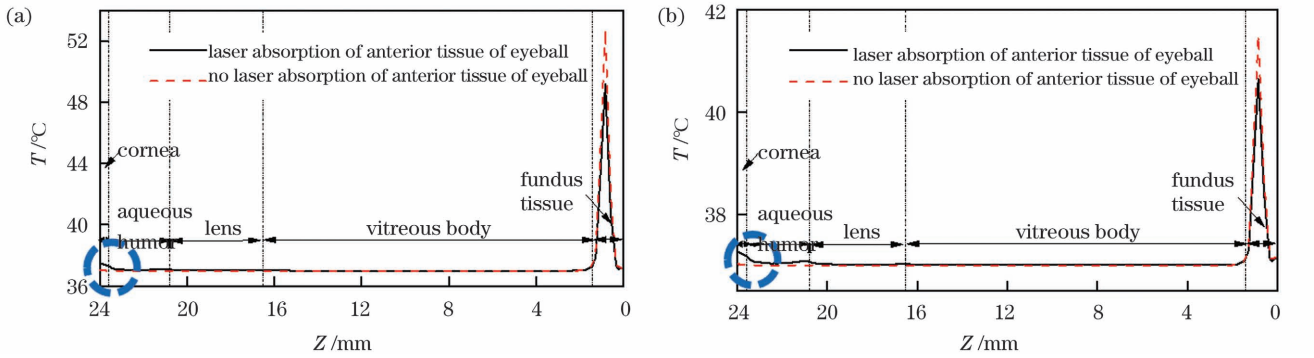

图 6 典型波长下，激光作用终了时眼球温度随瞳孔轴深度的变化(环境温度 T_a=35 ℃)。(a)λ=532 nm；(b)λ=810 nm

Fig. 6 Changes of eyeball temperature with pupillary axis at the end of laser treatment at typical wavelengths (ambient temperature T_a=35 ℃). (a) λ=532 nm ; (b) λ=810 nm

3.3 眼底血流灌注效应

脉络膜位于视网膜下方，主要由血管组成，其作用是为视网膜感光细胞提供营养。眼底激光手术中的全视网膜光凝主要用于治疗糖尿病视网膜病变等[22]。图 7 为全视网膜光凝下考虑和忽略脉络膜血流灌注时的温度分布。在全视网膜光凝手术中，选用的激光波长 λ=532 nm，入射能量密度 Q=5 J·cm^{-2}，激光脉宽 t_p=0.1 s，光束半径 r=200 μm。激光作用结束后，温升区域集中在眼底组织层内的激光光束区域内，如图中圆圈所示。由于激光作用时间短，考虑和忽略脉络膜血流灌注效应条件下眼球的温度峰值分别为 48.58 ℃和 48.63 ℃，差异较小。

与全视网膜光凝手术不同，经瞳孔温热疗法一般使用波长为 810 nm 的红外激光，采用较长的脉宽和较大的光斑，主要用于治疗脉络膜黑色素瘤等[23]。经瞳孔温热疗法中通常使用的激光参数为：激光波长 λ=810 nm，入射能量密度 Q=720 J/cm^2，激光脉宽 t_p=60 s，光束半径 r=1 mm。图 8 为激光作用终了(t=60 s)时全眼的温度分布。在经瞳孔温热疗法下，考虑和忽略脉络膜血流灌注效应时眼底的温度峰值分别为 48.54 ℃和 58.15 ℃，温升分别为 11.54 ℃和 21.15 ℃，误差为 83%(二者温升的差值与考虑脉络膜血流灌注效应时温升的比值)。

由上述分析可知，脉络膜血流灌注效应对激光手术中眼球温度分布的影响主要取决于激光脉宽：脉宽较短时(t_p=0.1 s)，血流灌注对眼底组织无明显的冷却效果，可以忽略血流灌注项的影响；脉宽较长时(t_p=60 s)时，血流灌注对眼底组织的冷却效果明显，会显著影响眼底的温度变化，必须考虑血流灌注项的影响。

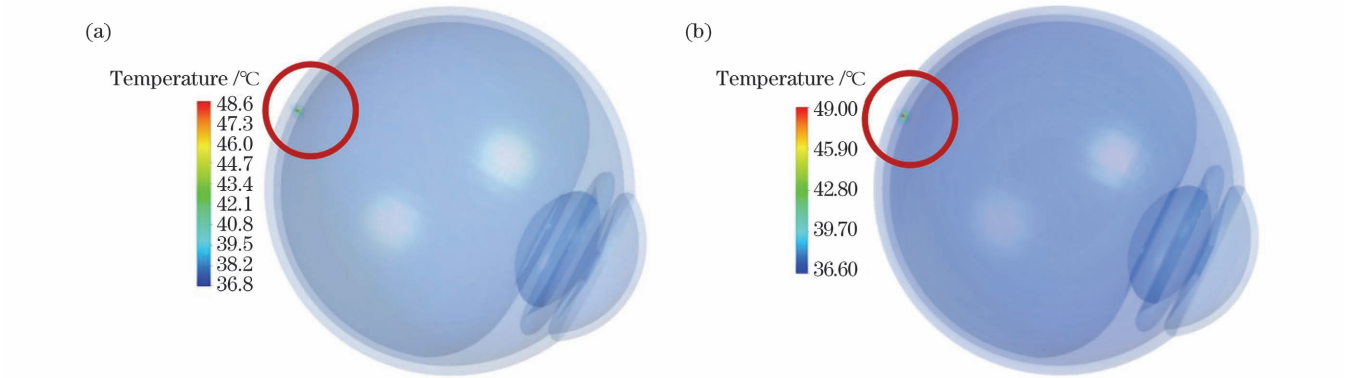

图 7 全视网膜光凝下激光作用终了时全眼的温度分布(t=0.1 s)。(a)考虑眼底血流灌注效应;(b)忽略眼底血流灌注效应

Fig. 7 Temperature distribution of whole eye after laser irradiation under whole retina photocoagulation (t=0.1 s). (a) Considering choroidal blood perfusion effect; (b) ignoring choroidal blood perfusion effect

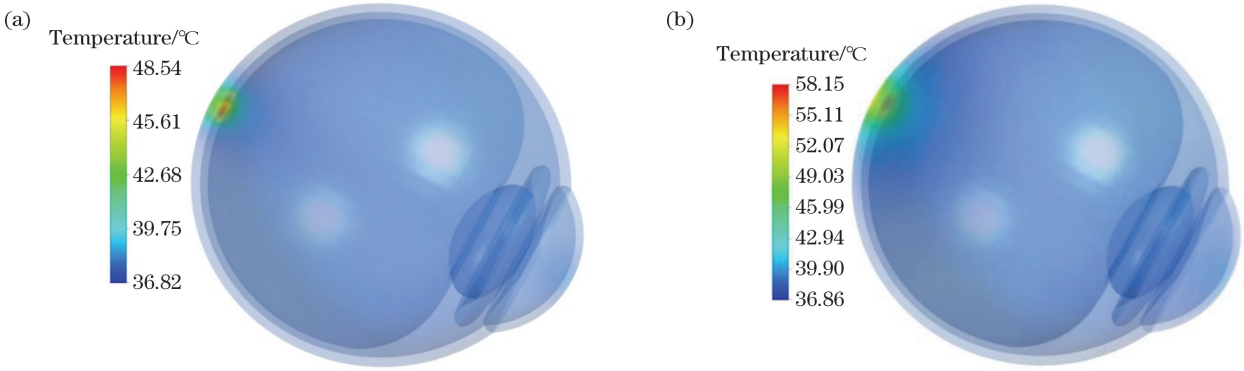

图 8 经瞳孔温热疗法激光作用终了时全眼的温度分布(t=60 s)。(a)考虑眼底血流灌注效应;(b)忽略眼底血流灌注效应

Fig. 8 Distribution of whole eye temperature after laser irradiation under transpupillary thermotherapy (t=60 s). (a) Considering choroidal blood perfusion effect; (b) ignoring choroidal blood perfusion effect

4 结 论

本团队基于真实眼部结构建立了全眼传热模型,计算了眼底激光手术传热过程,研究了环境温度、眼球前部组织光吸收和脉络膜血流灌注效应对眼球温度分布的影响。模拟结果表明:1)角膜与外部环境间的换热会导致眼球温度变化,其中眼球前部温度分布对环境因素较为敏感,而眼底组织受环境因素的影响较小,不会对眼底激光手术产生影响;2)在临床常用的 450~900 nm 波段内,若不考虑眼球前部四层组织对激光能量的吸收和散射作用,激光通量的误差高达 24%,引起的眼底各层温升误差可达 24%,会显著影响数值计算的准确性;3)脉络膜血流灌注项对激光手术中眼球温度分布的影响主要取决于脉宽。对于全视网膜光凝手术,由于激光作用时间短,考虑和忽略脉络膜血流灌注效应时眼球的温度峰值分别为 48.58 ℃和 48.63 ℃,差异较小;而对于经瞳孔温热疗法,考虑和忽略脉络膜血流灌注效应时眼球的温度峰值分别为 48.54 ℃和 58.15 ℃,温升分别为 11.54 ℃和 21.15 ℃,误差为 83%。

参 考 文 献

[1] Land M F. The human eye: structure and function[J]. Nature Medicine, 1999, 5(11): 1229-1269.

[2] Stewart M W. Treatment of diabetic retinopathy: recent advances and unresolved challenges[J]. World Journal of Diabetes, 2016, 7(16): 333-341.

[3] Campochiaro P A, Brown D M, Awh C C, et al. Sustained benefits from ranibizumab for macular edema following central retinal vein occlusion: twelve-month outcomes of a phase III study[J]. Ophthalmology, 2011, 118(10): 2041-2049.

[4] Jeong S H, Han J I, Cho S W, et al. Effect of focal laser photocoagulation in eyes with mild to moderate non-proliferative diabetic retinopathy[J]. International Journal of Ophthalmology, 2016, 9(10): 1439-1443.

[5] Fong D S, Girach A, Boney A. Visual side effects of successful scatter laser photocoagulation surgery for proliferative diabetic retinopathy: a literature review[J]. Retina, 2007, 27(7): 816-824.

[6] 黎黎, 张悦, 李萌茜, 等. 激光技术在眼科的应用现状与进展[J]. 中国激光, 2022, 49(5): 0507103.
Li L, Zhang Y, Li M X, et al. Current application and progress of laser technology in ophthalmology[J]. Chinese Journal of Lasers, 2022, 49(5): 0507103.

[7] 李治, 千维娜, 魏思敏, 等. 光热转换纳米材料在肿瘤光热治疗中的应用[J]. 激光与光电子学进展, 2020, 57(17): 170005.
Li Z, Qian W N, Wei S M, et al. Application of photothermal conversion nanomaterials in tumor photothermal therapy[J]. Laser & Optoelectronics Progress, 2020, 57(17): 170005.

[8] 辛坤, 史晓凤, 张旭, 等. 基于光热效应实现金纳米粒子的聚集及其 SERS 应用[J]. 光学学报, 2020, 40(19): 1930001.
Xin K, Shi X F, Zhang X, et al. Aggregation of gold nanoparticles based on photothermal effect and its application in surface-enhanced Raman scattering[J]. Acta Optica Sinica, 2020, 40(19): 1930001.

[9] Lee J G, Rosen R. Panretinal photocoagulation (PRP)[M].

Cham: Springer, 2017.
[10] Taflove A, Brodwin M E. Computation of the electromagnetic fields and induced temperatures within a model of the microwave-irradiated human eye[J]. IEEE Transactions on Microwave Theory and Techniques, 1975, 23(11): 888-896.
[11] Emery A F, Kramar P, Guy A W, et al. Microwave induced temperature rises in rabbit eyes in cataract research[J]. Journal of Heat Transfer, 1975, 97(1): 123-128.
[12] Ng E, Ooi E H, Acharya U R. FEM simulation of ocular surface temperature with bioheat equation[J]. IFMBE Proceedings, 2007, 14: 66-68.
[13] Cvetković M, Poljak D, Peratta A. Fetd computation of the temperature distribution induced into a human eye by a pulsed laser[J]. Progress in Electromagnetics Research, 2011, 120: 403-421.
[14] Narasimhan A, Jha K K, Gopal L. Transient simulations of heat transfer in human eye undergoing laser surgery[J]. International Journal of Heat and Mass Transfer, 2010, 53(1/2/3): 482-490.
[15] Heussner N, Holl L, Nowak T, et al. Prediction of temperature and damage in an irradiated human eye: utilization of a detailed computer model which includes a vectorial blood stream in the choroid[J]. Computers in Biology and Medicine, 2014, 51: 35-43.
[16] Welch A J, Pearce J A, Diller K R, et al. Heat generation in laser irradiated tissue[J]. Journal of Biomechanical Engineering, 1989, 111(1): 62-68.
[17] Karampatzakis A, Samaras T. Numerical modeling of heat and mass transfer in the human eye under millimeter wave exposure[J]. Bioelectromagnetics, 2013, 34(4): 291-299.
[18] Joukar A, Nammakie E, Niroomand-Oscuii H. A comparative study of thermal effects of 3 types of laser in eye: 3D simulation with bioheat equation[J]. Journal of Thermal Biology, 2015, 49/50: 74-81.
[19] Mirnezami S A, Rajaei J M, Abrishami M. Temperature distribution simulation of the human eye exposed to laser radiation[J]. Journal of Lasers in Medical Sciences, 2013, 4(4): 175-181.
[20] Heussner N, Stork W. Damage evaluation of the human eye for different laser sources-connecting ray tracing and finite volume calculations[J]. Journal of Medical and Bioengineering, 2015, 4(6): 475-479.
[21] Gokul K C, Gurung D B, Adhikary P R. FEM approach for transient heat transfer in human eye[J]. Applied Mathematics, 2013, 4(10): 30-36.
[22] Okamoto M, Matsuura T, Ogata N. Effects of panretinal photocoagulation on choroidal thickness and choroidal blood flow in patients with severe nonproliferative diabetic retinopathy[J]. Retina, 2016, 36(4): 805-811.
[23] Reichel E, Berrocal A M, Ip M, et al. Transpupillary thermotherapy of occult subfoveal choroidal neovascularization in patients with age-related macular degeneration[J]. Ophthalmology, 1999, 106(10): 1908-1914.

Numerical Simulation of Heat Transfer in Fundus Laser Surgery

Zhao Penghui[1], Zhao Yibo[1], Li Dong[1*], Chen Bin[1], Yao Liang[2**]

[1] *State Key Laboratory of Multiphase Flow in Power Engineering, Xi'an Jiaotong University, Xi'an* 710049, *Shaanxi, China*;
[2] *Department of Ophthalmology, the Second Affiliated Hospital of Xi'an Jiaotong University, Xi'an* 710004, *Shaanxi, China*

Abstract

Objective Fundus disease has been listed as one of the top three blinding eye diseases by the World Health Organization, accounting for 54.7% of all blinding eye diseases, and is the leading cause of blindness in the elderly. Traditional surgical methods are difficult to implement because the fundus is located behind the eyeball. Laser hyperthermia is the first choice for many retinal diseases. However, the probability of photoreceptor cell damage due to improper selection of laser parameters can be over 50%. Constructing an accurate three-dimensional heat transfer model of the entire eye will allow clinicians to select laser parameters. Therefore, a macroscopic heat transfer model of the entire eye was established on the basis of the real structure, and the effects of the external environment of the eye, anterior tissue absorption, and choroidal hemoperfusion on the fundus temperature distribution during laser surgery were analyzed using numerical simulation.

Methods A whole eye numerical model based on the Pennes' biological heat transfer equation was developed to calculate the thermal response process in the eyeball under steady state and laser heating in this paper. First, the fundamental properties of each region were strictly defined, including the external environment of the cornea, the initial temperature of the eyeball, and the setting of boundary conditions. The steady-state temperature distribution of the entire eye was solved by utilizing Pennes' biological heat transfer equation. The steady-state calculation results were then employed as the initial conditions to further solve the transient eye temperature distribution by changing the wavelength, pulse width, and energy density of the laser.

Results and Discussions In this study, the whole eye heat transfer model was established on the basis of real structure, the heat transfer process of fundus laser surgery was calculated, and the effects of ambient temperature, the light absorption of the anterior tissue of the eyeball, and choroid hemoperfusion on the temperature distribution in the eyeball were studied. The simulation findings showed that: 1) the heat transfer between the cornea and the external environment can change the temperature of the eyeball. The temperature distribution of the anterior eyeball is more sensitive to environmental factors, whereas the fundus tissue is less affected; thus, fundus laser surgery will not be

affected (Fig. 5). 2) If the absorption and scattering of laser energy by the four layers of anterior eyeball tissue are not considered, the maximum errors of fundus temperature rise were 24% and 56%, respectively, in the common clinical wavelength of 450–900 nm, which significantly affects the accuracy of numerical calculation (Fig. 6). 3) The effect of choroid perfusion term in ocular temperature distribution in laser surgery mainly depends on pulse width. Because of the short laser action time, the peak temperatures of the eyeball were 48.58 ℃ and 48.63 ℃ when the choroidal blood perfusion effect was considered or ignored, respectively, with little difference. However, when the effect of choroid perfusion was considered or ignored, the peak values of eyeball temperatures were 48.54 ℃ and 58.15 ℃ (Fig. 7 and Fig. 8), respectively, and the temperature rise was 11.54 ℃ and 21.15 ℃, respectively, with an error of 83%.

Conclusions Through theoretical research, the heat transfer process of fundus surgery under laser irradiation was analyzed from the macroscopic viewpoint in this report. The results indicated that the heat transfer between the cornea and the external environment could change intraocular temperature. The temperature distribution in the anterior part of the eyeball was more sensitive to the environmental factors, whereas the fundus tissue was less affected; thus, the fundus laser surgery would not be affected. The absorption and scattering of laser energy by the anterior tissue of the eyeball should be considered in the simulation to ensure the accuracy of the simulation of laser fundus surgery. The effect of choroidal blood perfusion on ocular temperature distribution in laser surgery was primarily determined using the laser pulse width. When the pulse width time was short (t_p = 0.1 s), hemoperfusion had no obvious cooling effect on fundus tissues, and the influence of perfusion factors could be ignored. Flow perfusion had a significant cooling effect on fundus tissues and significantly affected fundus temperature when the pulse width was long (t_p = 60 s). Therefore, the influence of perfusion factors must be considered. The results of this study provide important theoretical guidance for the clinical laser treatment of fundus diseases.

Key words medical optics; laser; fundus disease; photothermal effect; biological heat transfer; blood perfusion